Applied Clay Science 254 (2024) 107373

Contents lists available at ScienceDirect

Applied Clay Science

journal homepage: www.elsevier.com/locate/clay

Technical note

Preparation and release of antibacterial Na-mica-4/chlorhexidine nanocomposites

Luís H. Oliveira [a], Idglan S. de Lima [a], Denise B. França [a], Alan I.S. Moraes [a], Maria G. Fonseca [b], Humberto M. Barreto [c], Santiago Medina-Carrasco [d], Josy A. Osajima [a], Edson C. da Silva-Filho [a], María del Mar Orta [e,*]

[a] LIMAV, Interdisciplinary Laboratory of Advanced Materials, UFPI, 64049-550 Teresina, PI, Brazil
[b] LACOM, Laboratory of Fuels and Materials, UFPB, 58051-085 João Pessoa, PB, Brazil
[c] LPM, Laboratory of Research in Microbiology, UFPI, 64049-550 Teresina, PI, Brazil
[d] X-Ray Laboratory (CITIUS), Universidad de Sevilla, Avenida Reina Mercedes, 4B, 41012 Sevilla, Spain
[e] Analytical Chem. Dep. Pharmacy Fac. Sevilla Univ., C/ Profesor García González 2, 41012 Sevilla, Spain

ARTICLE INFO

Keywords:
Antibacterial activity
Chlorhexidine digluconate
High charge swelling mica

ABSTRACT

High charge swelling micas are layered silicates used in adsorption of several inorganic and organic species. In this study, we evaluated the adsorption of chlorhexidine digluconate on highly charge mica Na-mica-4. Drug release and antibacterial action against *Staphylococcus aureus* (*S. aureus*) and *Escherichia coli* (*E. coli*) using the direct contact test for mica/chlorhexidine hybrids were evaluated. The hybrids were characterized using X-ray diffraction, Fourier transform infrared spectroscopy, zeta potential measurements, CHN elemental analysis, and scanning electron microscopy. Chlorhexidine interacts successfully with the mica surface. The maximum amount of chlorhexidine incorporated was 583 mg g^{-1}, and the characterizations indicated that electrostatic attraction between the protonated amino group of the drug and the negative surface of clay was predominant in the formation of hybrids. Release kinetics study indicated that 80% of the drug release occurred in the first 12 h. The antibacterial test proved to be dependent on the time of chlorhexidine release, reaching 100% inhibition against *S. aureus* and *E. coli* after 0.5 h and 6 h, respectively.

1. Introduction

Microbial resistance has become a worldwide concern due to the possible complications to human and animal health that these microorganisms can cause (Yu et al., 2020). Recently, nanotechnology has become one of the emerging technologies in the field of drug delivery for the treatment of infectious diseases (Saadat et al., 2022). Therefore, the use of pharmacological molecules that can act against these microorganisms and consequently be able to replace or at least reduce the use of antibiotics has been studied (de Oliveira et al., 2022; Oliveira et al., 2023; S. C. Wu et al., 2019), and among them stands out chlorhexidine (de Oliveira et al., 2023a; Kathuria et al., 2021). Chlorhexidine (CHX) is a bivalent cationic biguanide molecule with high activity against gram-positive and gram-negative bacteria and fungi (de Oliveira et al., 2023a; Kathuria et al., 2021). Due to its cationic nature, chlorhexidine is attracted to anionic residues present on the bacterial surface and is adsorbed on the cytoplasmic membrane by electrostatic interactions, thus increasing its permeability, resulting in extravasation of low molecular weight microbial components, leading to lysis and death (de Oliveira et al., 2023a; Kathuria et al., 2021; Williamson et al., 2017).

However, the uncontrolled and rapid release of chlorhexidine formulations becomes the main disadvantage of using this molecule as an antibacterial agent, especially in prolonged applications (Brookes et al., 2020). As an alternative, chlorhexidine-controlled release systems have been carried out, mainly using clay minerals as a release vehicle (de Oliveira et al., 2023a).

Clay minerals stand out due to their high absorbability and swelling capacity (Saadat et al., 2022). Furthermore, the adsorption/incorporation of chlorhexidine in clay minerals, such as montmorillonite (de Oliveira et al., 2023a; Sun et al., 2018; Wu et al., 2013), kaolinite (Bardoňová et al., 2020; Isah et al., 2020; Jou and Malek, 2016) and vermiculite (Holešová et al., 2010, 2014; Samlíková et al., 2017) can

* Corresponding author.
E-mail address: enmaorta@us.es (M.M. Orta).

https://doi.org/10.1016/j.clay.2024.107373
Received 29 November 2023; Received in revised form 8 April 2024; Accepted 12 April 2024
Available online 16 April 2024

provide stability to this molecule. However, for natural clay minerals, they may have impurities such as quartz, which may reduce the use of these materials for medicinal purposes. However, for natural clay minerals, they may have impurities such as quartz, which may reduce the use of these materials for medicinal purposes (Carretero et al., 2006). In this way, the high-purity synthetic Na-mica-4 stands out.

Na-mica-x micas are 2:1 silicate, with a high exchange capacity. These fluoromicas have an ideal formula of $Na_n(Si_{8-n}Al_n)(Mg_6)O_{20}F_4$, with a trioctahedral structure that has only Si^{4+} and Al^{3+} cations in the tetrahedral sheets, Mg^{2+} cations in the octahedral sites and groups F^- on its edges (Osuna et al., 2019a; Osuna et al., 2019b; Taruta et al., 2022). This clay has a negative charge counterbalanced by Na + ions, resulting in CEC between 245 and 468 cmol(+)/kg, derived from isomorphic substitution in the tetrahedral site, which provides layer charge of 2, 3 or 4 (Osuna et al., 2021; Osuna et al., 2019a).

Na-mica-x synthetic micas have been successfully used in the adsorption/incorporation of medicines, including anti-inflammatory such as ibuprofen (Martín et al., 2019) and diclofenac (Martín et al., 2018); for abnormal blood lipid levels such as gemfibrozil (Martín et al., 2018), anticonvulsant medication such as carbamazepine (Martín et al., 2018); and hypertension such as propranolol (Martín et al., 2018). However, the use of Na-mica-x in the adsorption/incorporation and release of drugs with potential antibacterial action, such as chlorhexidine has not been investigated.

Thus, the aim of this work is to study the formation of novel hybrids based on chlorhexidine and highly charged swelling synthetic mica (Na-mica-4). Furthermore, the CHX release kinetic profile of the mica/CHX hybrid in phosphate buffered saline at pH 7.4 was study. Evaluation of the antibacterial action against Gram-negative bacteria, *E. coli*, and Gram-positive, *S. aureus*, were also investigated.

2. Experimental

2.1. Materials

SiO_2 with a 0.011 μm particle size, mean pore size of 60 Å, and a surface area 175–225 m^2/g (CAS: 112945–52-5, 99.8% purity), $Al(OH)_3$ (CAS: 21645–51-2), MgF_2 (CAS: 7783-40-6, 99% purity) and NaCl (CAS: 7647-14-5, 99.5% purity), chlorhexidine digluconate (CAS: 18472–51-0) and phosphate buffered saline pH = 7.4 (PBS), were purchased from Sigma-Aldrich. Brain Heart Infusion (BHI) agar and Muller-Hinton agar were purchased from Kasvi. Distillated water was used in all preparations.

2.2. Na-mica-4 synthesis

Na-mica-4 with ideal half formula $[Si_4Al_4]Mg_6O_{20}F_4{\cdot}nH_2O$ was synthesized following the procedure described by Alba et al. (2006). Based on the composition (8 - n) SiO_2, (n/2) Al_2O_3, 6MgF_2 and (2n) NaCl of the amount of SiO_2, $Al(OH)_3$, MgF_2 and NaCl, they were 2.40, 3.12, 3.74, 2.34 g, respectively. The chemicals were mixed in an agate mortar until a homogeneous mixture, and then the solid mixture was transferred to a platinum crucible and heated at 900 °C at a 10° min^{-1} heating rate and system was maintained for 15 h. The product was thoroughly washed with distilled water, solid fration recovered by filtration, dried in an oven and deagglomerated in an agate mortar. The cation exchange capacity of the material is 468 cmol(+)/kg^{-1} (Alba et al., 2006; Osuna et al., 2019b).

2.3. Adsorption of chlorhexidine (CHX) on Na-mica-4

The adsorption of CHX followed the previous procedure (de Oliveira et al., 2023a) with some modifications. Samples of 50 mg Na-mica-4 were suspended in 20 mL of chlorhexidine digluconate aqueous solution at 0.05–2% *v*/v concentrations and pH 6.5. The systems were stirred for 24 h at 25 °C. The final pH was maintained at 6.4 without any adjustment. The CHX-loaded micas were recovered by centrifugation and samples were washed with deionized water and dried at 60 °C for 24 h. The obtained hybrids were named mica/CHXx, where x corresponds to the chlorhexidine concentration used in the synthesis.

The amount of CHX incorporated was quantified by UV–Vis spectrophotometer at 254 nm according to the eq. 1.

$$Q_e = \frac{(C_i - C_f)}{m}.V \quad (1)$$

Where C_i and C_f are the initial and equilibrium CHX concentrations, V is the volume of drug solution and m is the mass of mica.

2.4. Characterizations

X-Ray Diffraction (XRD) analysis was performed using LABX-XDR 600 equipment (Shimadzu) with Cu-Kα (λ = 1.5406 Å) and operating at 2 kVA, 40 kV, and 30 mA. Scans were performed in the 2θ range between 3 and 80°. Fourier transform infrared (FT-IR) spectra of the samples were recorded using a Shimadzu IRPrestige-21 spectrometer over a range of 4000–400 cm^{-1} at a resolution of 4 cm^{-1} and 30 scans per run. For the Zeta potential, aqueous suspensions were made with 0.1 g L^{-1} of Na-mica-4 or hybrids with chlorhexidine and 0.1 mol L^{-1} of $NaNO_3$. The pH was adjusted to the necessary point with solutions of 0.1 mol L^{-1} HNO_3 or 0.1 mol L^{-1} NaOH. Zeta potential measurements were performed using a Malvern dynamic light scattering device (Zetasizer Nano-ZS90). Scanning electron microscopy (SEM) images of the samples were obtained using a field emission gun (FEG) microscope (TESCAN MIRA3 LMH) operating at an accelerating voltage of 30 kV, equipped with an energy-dispersive X-ray spectroscopy (EDS, Oxford Ultim Max 65) and an electron backscatter diffraction detector (EBSD, Oxford Symmetry). The plasma was generated under an argon atmosphere. Transmision electron microscopy (TEM) was performed using a Talos S200 FEI equipment. A voltage acceleration of 200 kV and a current of 4 nA in STEM were used to obtain HAADF images, and EDS was performed at 200 kV and a current of 200 pA. The elemental analysis (CHN) of the solids was performed using a Perkin-Elmer PE-2400 microelemental analyzer.

2.5. In vitro CHX release study

The *in vitro* test for the release of CHX from the hybrid mica/CHX1% was carried out according to a previous study (Meng et al., 2009), with some modifications. The CHX release test was carried out in phosphate buffer saline medium (PBS) at pH 7.4. Initially, 50 mg of the mica/CHX1% hybrid was dispersed in 50 ml of PBS solution at pH 7.4, agitated at 37 °C in an incubator at 150 rpm. At regular intervals (0.08–72 h) an aliquot of 5.0 mL was withdrawn and the same volume of PBS was immediately added to the system to keep the volume constant over time. Aliquots were analyzed to determine the amount of CHX by UV–Vis spectroscopy at 254 nm. The study was performed in triplicate. The corrected concentration of drug released was calculated according to the eq. 4 (Xu et al., 2009; Zhu et al., 2005).

$$C_c = C_t + \frac{V_a}{V_T}\sum_0^{t-1} C_t \quad (4)$$

where C_c is the corrected concentration at time t, C_t is the apparent concentration at time t, V_a is the volume of sample taken and V_T is the total volume of release medium.

The release was analyzed, and the kinetic profile involved was statistically investigated by the Excel add-in DDSolver applying specific mathematical calculations to models: First-Order (Polli et al., 1997), Higuchi (Higuchi, 1961), Korsmeyer-Peppas (Korsmeyer et al., 1983) and Peppas-Sahlin (Peppas and Sahlin, 1989), according to the Eqs. 5–8.

$$\text{Frist} - \text{Order } logF = log\ k + n\ log\ (t) \quad (5)$$

$$\text{Higuchi} : F = \text{k}\, H_t^{\frac{1}{2}} \quad (6)$$

$$\text{Korsmeyer–Peppas} : F = \text{k}\, \text{t}^{\text{n}} \quad (7)$$

$$\text{Peppas} - \text{Sahlin} : F = k_1 t^m + k_2 t^{2m} \quad (8)$$

where F corresponds to the fraction of the drug released at each time (t), n is the release coefficient, k the release kinetic constant, k_1 the contribution of Fickian diffusion, k_2 the contribution of relaxation to the release mechanism and m o Fickian diffusion coefficient.

2.6. Antibacterial activity

The antibacterial activity of mica Na-mica-4 and the chlorhexidine hybrid mica/CHX1% were evaluated against both Gram-negative (*Escherichia coli* ATCC 25922) and Gram-positive (*Staphylococcus aureus* ATCC 25923) strains by the direct contact method (Zheng and Zhu, 2003), with some modifications. Bacterial cultures were prepared by transferring the inoculum from the nutrient medium to Brain Heart Infusion Medium (BHI). Aliquots of 50 μL were transferred to tubes containing 3 mL of saline solution and incubated at 37 °C for 24 h. The standardized inoculum was successively diluted to a concentration of approximately 1.5×10^4 CFU mL^{-1} (Colony Forming Unit) for later use in antimicrobial assays.

To evaluate antibacterial activity, 1000 μL of aliquots from the mica/CHX1% hybrid release study at times 0.5, 2, 6, 12 and 24 h were dissolved in 1000 μL of saline (0.85% NaCl solution). As a control, the same aliquot was removed within 24 h in a similar delivery system containing Na-mica-4. The direct contact test was performed according to the previous procedure (Zheng and Zhu, 2003). 100 μL of each aliquot solution of release/saline was added to a plate containing Muller-Hinton agar medium, after the addition of 100 μL of the standardized bacterial suspension. Then, plates were seeded using the spread plate method and incubated at 37 °C for 24 h. As a control, 100 μL of the bacterial suspension and 100 μL of saline were seeded, using the spread plate method, in plates with culture medium. All tests were performed in triplicate. The inhibitory effect of each solution was calculated using eq. (9).

$$n(\%) = \frac{N_1 - N_2}{N_1} x100 \quad (9)$$

Where n (%) is the percentage of inhibitory effect, N_1 is the ratio of the number of CFU that grew in the control plates and N_2 is the ratio of the number of CFU that grew in the plates containing the bacterial suspension and the test solution.

2.7. Statistical analysis

Antibacterial activity assays were performed in triplicate and the results normalized by calculating the arithmetic mean and standard deviation values using Microsoft Excel software.

3. Results and discussion

3.1. Adsorption of chlorhexidine on mica Na-mica-4

The results of the amount of CHX adsorbed on Na-mica-4 are shown in Table 1. The amount of adsorbed CHX increases with increasing concentration in each system, with a maximum amount of adsorbed CHX of 583 mg g^{-1}, indicating a good interaction between both species. The value corresponds to 1.15 of the mica CEC. Furthermore, it was observed that from the mica/CHX1% sample the amount of adsorbed CHX remains constant.

Furthermore, the amount of adsorbed CHX was also quantified by elemental analysis CHN and results are present in Table 1. The amount of nitrogen and carbon increased as a function of the CHX concentrations. For example, the nitrogen content increased from 2.0 (1.4 mmol g^{-1}) to 16.2% (11.4 mmol g^{-1}) by using 0.05% and 2% v/v concentrations in the preparations, indicating a good interaction between CHX and mica.

By CHN elemental analysis, the amount of organic groups (**q**) present in the materials was estimated considering that the CHX molecule has 10 nitrogen atoms (Oliveira et al., 2023). In this case, the amount of incorporated CHX increased as a function of the initial CHX concentration, and the values are in good agreement with the CHX amount quantified by UV–Vis.

3.2. XRD

The XRD patterns of Na-mica-4 and the mica/CHX hybrid are shown in Fig. 1. For Na-mica-4, the *001* reflection of the mica was observed at 2θ equal to 7.24°, corresponding to a d distance (d_{001}) of 1.21 nm, indicating the presence of a pseudo-monolayer of water in the interlayer spacing of clay mineral (Alba et al., 2006; Osuna et al., 2021; Osuna et al., 2019a; Pazos et al., 2012). Other reflections at 14.6°, 19.3°, 24.5°, 29.3°, 34.0°, 34.9°, 35.7°, 43.5°, 60.0° were indexed to mica phase (Alba et al., 2006). After CHX adsorption, the d_{001} values were maintained at 1.21 nm, suggesting that CHX molecule was not intercalated in the interlayer space of the mica, and that possible interaction between species on external surface of the clay minerals. CHX is a bisguanide with pK_{a1} 10.3 and pK_{a2} 2 (Agarwal et al., 2012; Ambrogi et al., 2017). Under the conditions of synthesis, the pH before and after adsorption was 6.5 ± 0.1. At pH 6.5, CHX is predominantly dicationic (100%) (Fig. SM1 (Ambrogi et al., 2017; de Oliveira et al., 2023a), −figure, tables or text in SM can be found online-). Furthermore, changes in the surface charge of the mica/CHX samples were followed by measurements of the Zeta potential and the results are present in Fig. 1(ii). Alterations in the Zeta potential were observed as a function of the CHX concentrations used in the preparations. For example, mica/CHX1% sample presented a zero-charge potential (pHpcz) at 7.61. This behavior was observed for interaction of other cationic molecules with Na-mica-4 such as chitosan (Alba et al., 2019), octadecylamine (Martín et al., 2019), and primary alkylammonium salt dodecylamine (del Orta et al., 2018), in addition to

Table 1
CHX adsorption on Na-mica-4 at pH 6.5, 25 °C and 50 mg adsorbent dosage, and elemental analysis, in percentages and mmol g^{-1}, of carbon (C), hydrogen (H), nitrogen (N) and organic groups (**q**) for mica/CHX hybrids.

Samples	CHX adsorbed		C		H	N		**q**
	mg g^{-1}	mmol g^{-1}	%	mmol g^{-1}	%	%	mmol g^{-1}	mmol g^{-1}
Na-mica-4	–	–	–	–	–	–	–	–
mica/CHX0.05%	76 ± 5	0.15 ± 0.01	4.2	3.5	0.78	2.0	1.4	0.14 ± 0.01
mica/CHX0.1%	116.7 ± 7	0.23 ± 0.01	5.5	4.6	1.70	2.8	2.0	0.20 ± 0.01
mica/CHX0.3%	195.6 ± 7	0.38 ± 0.01	8.0	6.70	2.51	5.2	3.7	0.37 ± 0.01
mica/CHX0.5%	297 ± 6	0.58 ± 0.01	12.4	10.3	2.43	8.0	5.7	0.57 ± 0.01
mica/CHX0.7%	404 ± 8	0.79 ± 0.02	14.8	12.3	2.85	11	7.7	0.77 ± 0.02
mica/CHX1%	574 ± 7	1.13 ± 0.01	21.4	17.8	2.88	15.4	11	1.10 ± 0.01
mica/CHX1.5%	579 ± 5	1.14 ± 0.01	22.2	18.5	2.09	15.9	11.3	1.13 ± 0.02
mica/CHX2%	583 ± 3	1.15 ± 0.01	22.7	18.9	2.75	16.2	11.4	1.14 ± 0.02

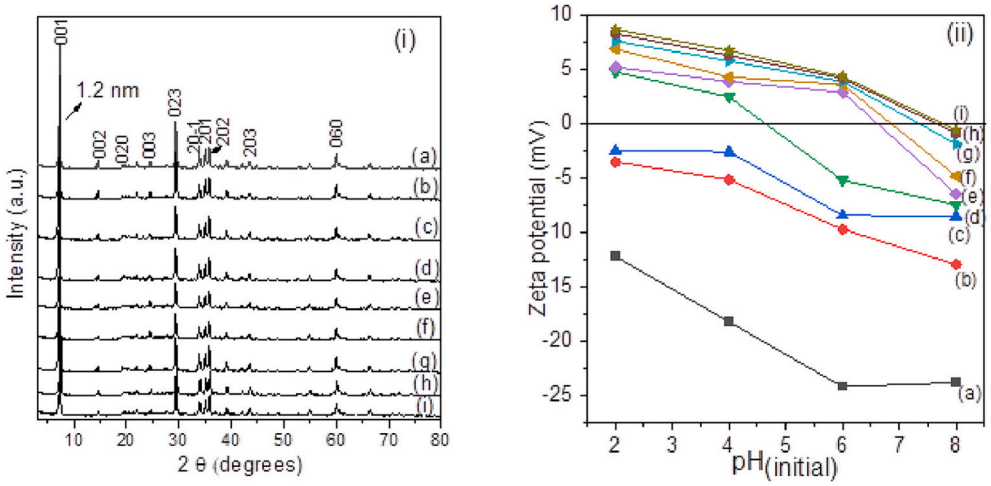

Fig. 1. (i) XRD patterns and (ii) Zeta potential measurements of (a) hybrid Na-mica-4 and mica/CHX hybrid (b) mica/CHX0.05%, (c) mica/CHX0.1%, (d) mica/CHX0.3%, (e) mica/CHX0.5%, (f) mica/CHX0.7%, (g) mica/CHX1%, (h) mica/CHX1.5% and (i) mica/CHX2%;

the interaction of CHX with montmorillonite (Oliveira et al., 2023).

Thus, possibly the main mechanism of interaction in the formation of Na-mica-4/CHX hybrids is between the protonated amine groups of CHX and the negative external surface of Na-mica-4, as proposed in Fig. 2.

3.3. FTIR spectroscopy

The FTIR spectra of the mica samples before and after CHX adsorption are shown in Fig. 3. The FTIR spectrum of the Na-mica-4 sample presents a broad absorption at 3477 and a sharp band at 1648 cm^{-1} associated with OH stretching and vibration of deformation in water, respectively (Alba et al., 2019; Osuna et al., 2020). Furthermore, bands at 950, 824, 684 and 468 cm^{-1} were attributed to Si-O-Si and Si-O-Al stretchings and Si-O-Al deformation, respectively (Madejová et al., 2017; Osuna et al., 2020).

After CHX adsorption, new bands were observed in all spectra of the hybrids. The absorptions at 3200, 2940 and 2850 cm^{-1} were attributed to the N—H stretching and to the antisymmetric and symmetric CH stretchings, respectively (Lin-Vien et al., 1991; Saha et al., 2014; Yang et al., 2007). Absorptions at 1586 and 1536 cm^{-1} were assigned to C═C stretching (De Oliveira et al., 2023b; Pal et al., 2009). The bands at 1488 and 1417 cm^{-1} were assigned to C-N-H vibrations (Lin-Vien et al., 1991; Onnainty et al., 2016). The absorption at 1250 cm^{-1} was related to the C—N stretching (Lin-Vien et al., 1991; Y. Wu et al., 2013). OH stretching band was dislocated to lower wavenumber, suggesting possible interaction between the OH surface and the groups of the CHX.

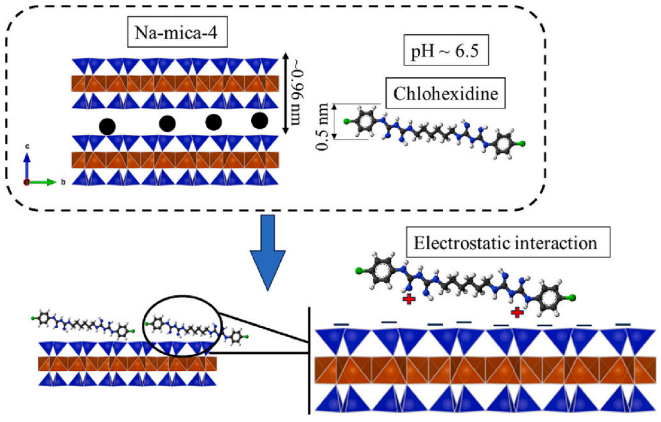

Fig. 2. Illustrative scheme for the proposed interaction between chlorhexidine and Na-mica-4 at pH 6.5.

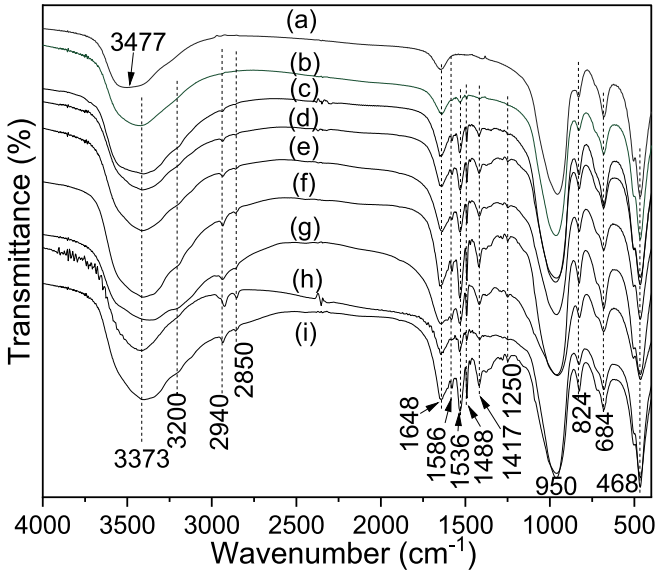

Fig. 3. FTIR spectra for (a) Na-mica-4, and mica/CHX hybrids (b) mica/CHX0.05%, (c) mica/CHX0.1%, (d) mica/CHX0.3%, (e) mica/CHX0.5%, (f) mica/CHX0.7%, (g) mica/CHX1%, (h) mica/CHX1.5%, and (i) mica/CHX2%.

3.4. Scanning electron microscopy (SEM)

SEM images of the Na-mica-4 samples and the mica/CHX hybrids are shown in Fig. 4. For Na-mica-4, a plate-like morphology characteristic of micas was observed in Fig. 4(a) (Komarneni et al., 1999; Park et al., 2002).

For CHX loaded samples, the same morphological profile was observed in all samples. However, some disorganised plates were observed with the increase in the CHX concentration with small changes in morphology. For example, with increasing chlorhexidine concentration, a finer structure was observed, in addition to smaller particles distributed in the larger particles. This fact is more evident in the mica/CHX0.7% to mica/CHX2% hybrids.

TEM images of the samples, Na-mica-4 and after the reaction with chlorhexidine at the highest concentration, mica/CHX2%, are shown in Figures SM2 and SM3, respectively. In both images, it was observed that the plate structure of the clays was maintained. However, for the sample with chlorhexidine, small particles were observed. In the elemental

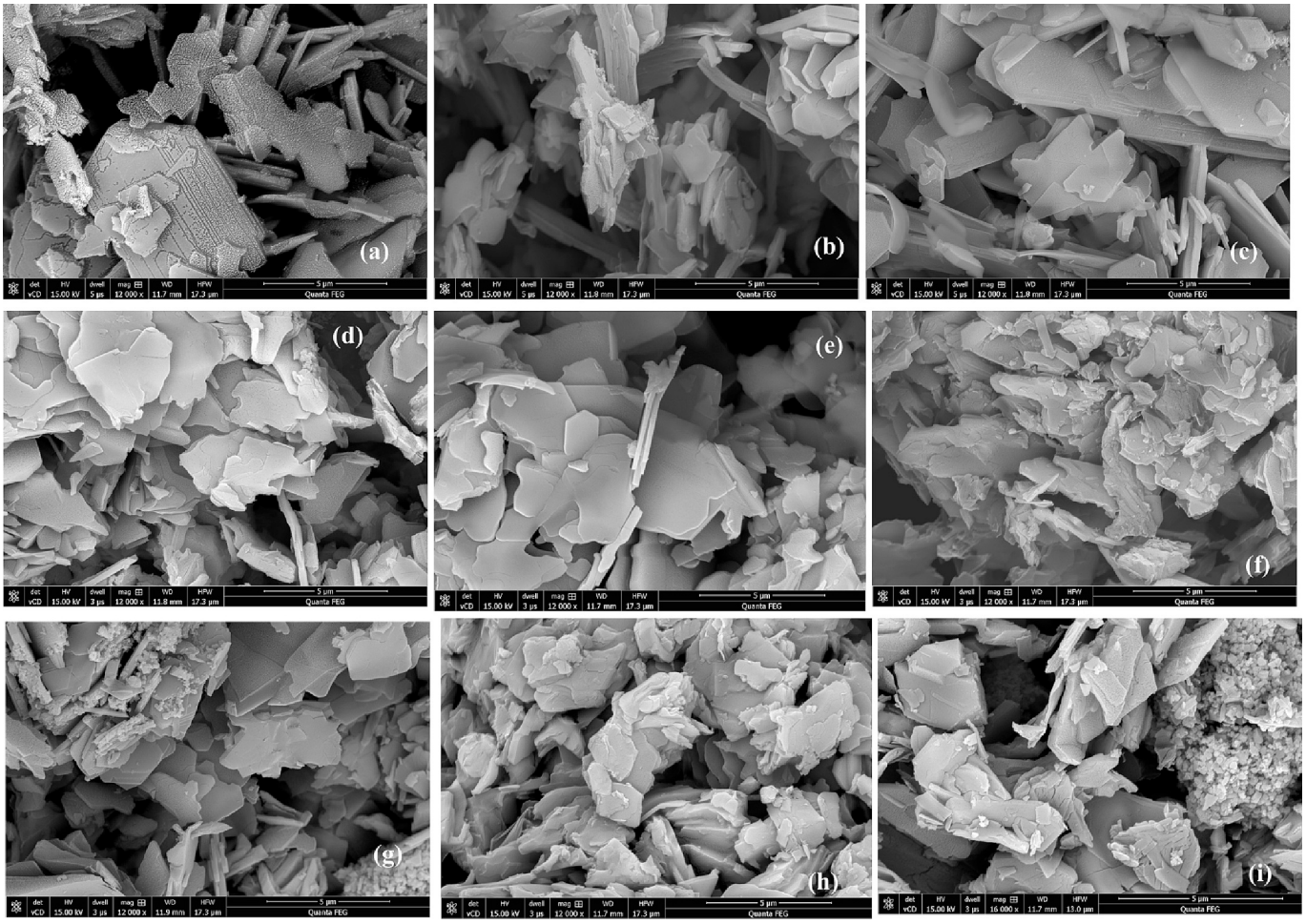

Fig. 4. SEM images of (a) Na-mica-4 and mica/CHX hybrids (b) mica/CHX0.05%, (c) mica/CHX0.1%, (d) mica/CHX0.3%, (e) mica/CHX0.5%, (f) mica/CHX0.7%, (g) mica/CHX1%, (h) mica/CHX1.5% and (i) mica/CHX2%.

mapping of these samples, Figure SM2 and SM3, the presence of the elements Si, O, Al, Na, Mg and F were observed for both samples, differing, however, in the presence of the element C in the sample with chlorhexidine, indicating the presence of this drug in the sample.

3.5. *In vitro drug release study*

Solid prepared at intermediate concentration of CHX was selected for the drug release and the CHX release profile is shown in Fig. 5. CHX was released over a period of 72 h, reaching approximately 80% in the first 12 h. This fact may be associated with the drug interaction site in the clay. CHX adsorption on highly charged synthetic mica occurred on the external surface of the clay mineral, as observed in the XRD results. Thus, the high release rate (~80%) in the first 12 h is associated with the interaction of CHX on the outer surface of the mica, which may have facilitated drug release. In the following hours, ~10% more CHX was released more continuously and slowly, totaling approximately 90% in 72 h. The current data were compared with CHX release studies based on some clay minerals, such as montmorillonite and palygorskite, Table 2. In general, for montmorillonite, CHX adsorption occurs at two possible sites involving the outer surface and the inner surface (interlayer space) (Meng et al., 2009; Oliveira et al., 2023; Saha et al., 2014), which may occur an initial drug burst, for those pharmacological molecules that interacted on the external surface of the clay mineral, and then a slower and controlled release of the drug present in the interlayer space.

The kinetic profile of the mica/CHX1% hybrid was fitted to the first order, Higuchi, Korsmeyer-Peppas and Peppas-Sahlin models, and data

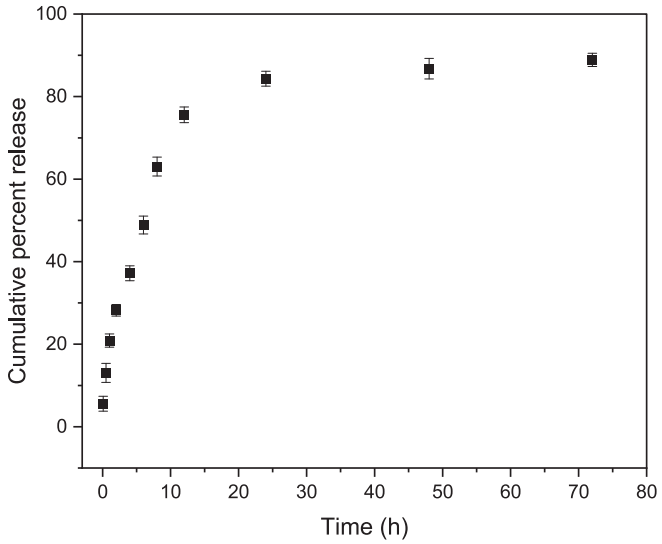

Fig. 5. CHX release profile from mica/CHX1% in PBS medium at pH 7.4 and 37 °C.

are described in Table SM1. The model that best described the experimental data was Peppas-Sahlin model, with a correlation coefficient of 0.964. This model may indicate that the release mechanism can occur by

Table 2
Systems based on CHX and clays for CHX release.

System of CHX release	Experimental conditions for drug release	Results	Ref
Mt/CS/CHX bionanacomposite	Conducted at room temperature with the dialysis bag at pH 1.2 (0.1 M HCl), 4.2 and 6.8 (mixing acetic acid: sodium acetate)	The release of CHX from Mt./CS/CHX after 24 h at pH 1.2, 4.2 and 6.8 was ~35%, ~30% and ~ 20%, respectively.	(Onnainty et al., 2016)
CHX/Mt. and CHX/Mt./CS film	The *in vitro* release of CHX from films was carried out for 48 h with a Franz diffusion cell at 37 °C using saline solution (8.29 g of NaCl and 0.27 g of $CaCl_2$ in 1000 mL solution)	After a moderate burst effect with a 25% of CHX released, the film based on CHX/mt/CS it continued slowly and did not reach a 50% of release either after 24 h.	(Ambrogi et al., 2017)
CHX-Cu/Mt. nanocomposite	The release was carried out in 0.9% saline solution by using a dialysis bag technique	CHX–Cu complexes were released continuously over 288 h and 16% of total CHX–Cu complexes were released. In the initial 6 h, approximately 6% of the CHX-Cu complexes were released burstly from the surface of Mt.	(Wu et al., 2013)
Palygorskite/CHX and Mt./CHX	The release was carried out in PBS media (pH = 7.3) during 24 h at 37 °C.	Drug release kinetic in PBS media shows a continuous release over 25 h for both systems (Mt and Pal), existing a burst release in the first 5 h.	(Lobato-Aguilar et al., 2018)
		Both materials show a release within 24 h, containing an initial burst-like release in the first 5 h continuing with a more sustained release for the next 19 h.	(Lobato-Aguilar et al., 2020)
CHX/Mt	*In vitro* release studies were carried out in PBS media of pH 7.4 using the dialysis bag at 37 °C.	CHX was continuously released over 72 h and burst release of CHX was observed for initial 24 h.	(Meng et al., 2009)
Lap-APTES/CHX	The release was conducted by using deionized water at pH 7.2 and 25 °C.	In water, the CHX release rate was constant up to 8 h (total CHX release ~10%). A plateau was not reached, which evidenced the very slow release of the drug within the first 24 h.	(Peraro et al., 2020)
CHX/Mt	The release was carried out in PBS media of pH 7.4 using the dialysis bag at 37 °C	Initial burst release lasted up 12 h, with a total drug released of 20%. After 180 h, the total drug released was 54%.	(Saha et al., 2014)
BisGMA/TEGDMA. /Cloisite 30B/ CHX	Disc shaped specimens of 5 mm diameter and 1 mm high were made only for the composites. The initial mass of the speciments was registered prior to immersion in 5 mL of 50 mM phosphate buffered saline solution (pH 7) at 37 °C.	The hybrid presented a CHX release of about 10–15% its initial content over time if compared during the experiment period.	(Boaro et al., 2019)
Halloysite/CHX	Drug release was investigated in deionized water at room temperature.	The composite showed a relatively sustained drug release profile; only 25% of CHX was released from nanotubes within the first hour	(Wu et al., 2017)
Mt/CHX and Mt./CHX/TBH	The dissolution test was performed using a shaker bath (SV1422, Schutzart, Germany) by suspending dialysis bags containing Mt./CHX (or Mt./TBH or Mt./CA/TBH) in 200 mL of 0.9 wt% NaCl solution at 37 °C.	Mt/CHX hybrid had a burst release of ~30% within the first 24 h	(Sun et al., 2018)

Mt: montmorillonite; CS: chitosan; Cu: copper; Pal: palygorskite; PBS: phosphate buffered saline; Lap: Laponite; APTES: 3-aminopropyl triethoxysilane; BisMGa: Bis(2-hydroxy-3-methacryloxypropyl)Ether; TEGDMA: Triethyleneglycol dimethacrylate TBH: terbinafine hydrochloride.

diffusion or by the relaxation of the polymeric chains, these models still obtain the values of K_1 and K_2, which represent the influence of diffusion and the polymeric relaxation, respectively. When K1 > K2, release occurs predominantly by diffusion (Peppas and Sahlin, 1989). In this study, the parameters obtained were K1 and K2 were 28.1 and − 2.18, respectively, indicating that the release of CHX from the mica/CHX1% hybrid occurred by diffusion.

3.6. Antibacterial assays

The antibacterial activity of chlorhexidine solutions and samples against *E. coli* and *S. aures* was evaluated by the direct contact method and the results are given in Table 3. The formation of bacterial colonies is observed on the plates, Figures SM4 and SM5, and a high number of bacterial colonies are observed on the control plates for both bacteria.

For chlorhexidine solutions at the same concentrations as used for hybrid preparation (1% *v*/v) exhibit 100% inhibition against both bacteria, (Figs. SM4 and SM5), indicating that both strains are sensitive to chlorhexidine at this concentration (de Oliveira et al., 2023a). However, the Na-mica-4 sample showed low antibacterial activity for both strains, with inhibition values of 18.45 and 17.8% against *E. coli* and *S. aureus*, respectively. Similar results were found for other clay minerals such as montmorillonite (de Oliveira et al., 2023a; Saha et al., 2014) and palygorskite (Lobato-Aguilar et al., 2020), indicating the low antibacterial activity of the pristine clay minerals against both strains tested.

Table 3
Inhibitory potential of samples Na-mica-4 at time 24 h and mica/CHX1% hybrids, at times 0.5 h, 2 h, 6 h, 12 h and 24 h against *E. coli* and *S. aureus*.

Sample	Time release (h)	Antibacterial action (% inhibition)	
		E. coli	*S. aureus*
Na-mica-4	24	18.4 ± 4	17.8 ± 3
mica/CHX1%	0.5	70 ± 8	100
	2	93 ± 6	100
	6	100	100
	12	100	100
	24	100	100

However, the release aliquots of the hybrid mica/CHX1% showed high antibacterial action against both tested strains. For example, the action against *E. coli*, from the release aliquot at 6 h, showed 100% inhibition. At the lower times of 0.5 and 2 h, approximately 70 and 95% inhibition were achieved, respectively. Compared to the bacteria *S. aureus*, the release aliquot at 0.5 h exhibited 100% inhibition. These results indicated the effective antibacterial action of the mica/CHX1% hybrid against both *E. coli* and *S. aureus* bacteria (Table 3). Similar results were found in montmorillonite/CHX hybrids (Oliveira et al., 2023; Sun et al., 2018) and kaolinite/CHX hybrids (Jou and Malek, 2016; Wu et al., 2017).

4. Conclusions

In this study, the adsorption of chlorhexidine digluconate at different concentrations on highly loaded synthetic mica, Na-mica-4, was investigated. Characterizations confirmed the interaction of the organic molecule on the external surface of the clay. The interaction between species possibly occurred by electrostatic interaction between the protonated amine groups of chlorhexidine and the negative surface of mica and between the OH surface of mica and the groups of the CHX. A high amount of chlorhexidine was adsorbed and release kinetics data indicated that the Peppas-Sahlin mode satisfied the release process. The antibacterial action of the mica/CHX hybrid was effective, reaching

100% inhibition against *E.coli* and *S. aures*.

CRediT authorship contribution statement

Luís H. Oliveira: Writing – original draft, Methodology. **Idglan S. de Lima:** Writing – original draft, Methodology. **Denise B. França:** Writing – original draft. **Alan I.S. Moraes:** Writing – original draft. **Maria G. Fonseca:** Writing – review & editing, Methodology. **Humberto M. Barreto:** Methodology. **Santiago Medina-Carrasco:** Methodology. **Josy A. Osajima:** Writing – review & editing, Methodology. **Edson C. da Silva-Filho:** Writing – review & editing, Supervision, Conceptualization. **María del Mar Orta:** Writing – review & editing, Supervision, Funding acquisition, Conceptualization.

Declaration of competing interest

The authors declare that they have no known competing financial interests or personal relationships that could have appeared to influence the work reported in this paper.

Data availability

No data was used for the research described in the article.

Acknowledgement

The authors, S.M.C. and M.M.O., acknowledge the University of Seville through the *VII* Plan Propio de Investigación by Proyect 2022/00000444, for the Constitution of Thematic Networks and by Proyect 2023/00000313 for Use of General Research Services and Fundación Carolina for providing financial support The authors, L.H.O., I.S.L, D.B.F., A.I.S.M., M.G.F., H.M.B., J. A.O. and E.C.S.F., would like to thank the funding agencies National Council for Scientific and Technological Development – CNPq, Research Support Foundation of Piauí – FAPEPI for providing financial support.

Appendix A. Supplementary data

Supplementary data to this article can be found online at https://doi.org/10.1016/j.clay.2024.107373.

References

Agarwal, A., Nelson, T.B., Kierski, P.R., Schurr, M.J., Murphy, C.J., Czuprynski, C.J., McAnulty, J.F., Abbott, N.L., 2012. Polymeric multilayers that localize the release of chlorhexidine from biologic wound dressings. Biomaterials 33 (28), 6783–6792. https://doi.org/10.1016/j.biomaterials.2012.05.068.

Alba, M.D., Castro, M.A., Naranjo, M., Pavón, E., 2006. Hydrothermal Reactivity of Na- n -Micas (n = 2, 3, 4). Chem. Mater. 18 (12), 2867–2872. https://doi.org/10.1021/cm0514802.

Alba, M.D., Cota, A., Osuna, F.J., Pavón, E., Perdigón, A.C., Raffin, F., 2019. Bionanocomposites based on chitosan intercalation in designed swelling high-charged micas. Sci. Rep. 9 (1), 1–9. https://doi.org/10.1038/s41598-019-46495-z.

Ambrogi, V., Pietrella, D., Nocchetti, M., Casagrande, S., Moretti, V., De Marco, S., Ricci, M., 2017. Montmorillonite–chitosan–chlorhexidine composite films with antibiofilm activity and improved cytotoxicity for wound dressing. J. Colloid Interface Sci. 491, 265–272. https://doi.org/10.1016/j.jcis.2016.12.058.

Bardoňová, L., Mamulová Kutláková, K., Kotzianová, A., Kulhánek, J., Židek, O., Velebný, V., Tokarský, J., 2020. Electrospinning of Fibrous Layers Containing an Antibacterial Chlorhexidine/Kaolinite Composite. ACS Appl. Bio Mater. 3 (5), 3028–3038. https://doi.org/10.1021/acsabm.0c00088.

Boaro, L.C.C., Campos, L.M., Varca, G.H.C., dos Santos, T.M.R., Marques, P.A., Sugii, M. M., Saldanha, N.R., Cogo-Müller, K., Brandt, W.C., Braga, R.R., Parra, D.F., 2019. Antibacterial resin-based composite containing chlorhexidine for dental applications. Dent. Mater. 35 (6), 909–918. https://doi.org/10.1016/j.dental.2019.03.004.

Brookes, Z.L.S., Bescos, R., Belfield, L.A., Ali, K., Roberts, A., 2020. Current uses of chlorhexidine for management of oral disease: a narrative review. J. Dent. 103 (July) https://doi.org/10.1016/j.jdent.2020.103497.

Carretero, M.I., Gomes, C.S.F., Tateo, F., 2006. Chapter 11.5 Clays and Human Health. In: Developments in Clay Science, 1, issue C, pp. 717–741. https://doi.org/10.1016/S1572-4352(05)01024-X.

de Oliveira, L.H., Trigueiro, P., Souza, J.S.N., de Carvalho, M.S., Osajima, J.A., da Silva-Filho, E.C., Fonseca, M.G., 2022. Montmorillonite with essential oils as antimicrobial agents, packaging, repellents, and insecticides: an overview. Colloids Surf. B: Biointerfaces 209, 112186. https://doi.org/10.1016/j.colsurfb.2021.112186.

de Oliveira, L.H., de Lima, I.S., dos Santos, A.N., Trigueiro, P., Barreto, H.M., Cecília, J. A., Osajima, J.A., da Silva-Filho, E.C., Fonseca, M.G., 2023a. Monitoring the antimicrobial activity of bentonite-chlorhexidine hybrid. Mater. Today Communicat. 34 (August 2022), 105352 https://doi.org/10.1016/j.mtcomm.2023.105352.

De Oliveira, L.H., De Lima, I.S., Adriana, N., Trigueiro, P., Barreto, H.M., Antonio, J., Osajima, J.A., Silva-filho, E.C., Fonseca, M.G., 2023b. Monitoring the antimicrobial activity of bentonite-chlorhexidine hybrid. Mater. Today Communicat. 34 (January), 105352 https://doi.org/10.1016/j.mtcomm.2023.105352.

del Orta, M.M., Martín, J., Medina-Carrasco, S., Santos, J.L., Aparicio, I., Alonso, E., 2018. Novel synthetic clays for the adsorption of surfactants from aqueous media. J. Environ. Manag. 206, 357–363. https://doi.org/10.1016/j.jenvman.2017.10.053.

Higuchi, T., 1961. Rate of Release of Medicaments from Ointment Bases Containing Drugs in Suspension. J. Pharm. Sci. 50 (10), 874–875. https://doi.org/10.1002/jps.2600501018.

Holešová, S., Valášková, M., Plevová, E., Pazdziora, E., Matějová, K., 2010. Preparation of novel organovermiculites with antibacterial activity using chlorhexidine diacetate. J. Colloid Interface Sci. 342 (2), 593–597. https://doi.org/10.1016/j.jcis.2009.10.051.

Holešová, S., Štembírek, J., Bartošová, L., Pražanová, G., Valášková, M., Samlíková, M., Pazdziora, E., 2014. Antibacterial efficiency of vermiculite/chlorhexidine nanocomposites and results of the in vivo test of harmlessness of vermiculite. Mater. Sci. Eng. C 42, 466–473. https://doi.org/10.1016/j.msec.2014.05.054.

Isah, M., Asraf, M.H., Malek, N.A.N.N., Jemon, K., Sani, N.S., Muhammad, M.S., Wahab, M.F.A., Saidin, M.A.R., 2020. Preparation and characterization of chlorhexidine modified zinc-kaolinite and its antibacterial activity against bacteria isolated from water vending machine. J. Environ. Chem. Eng. 8 (2), 103545 https://doi.org/10.1016/j.jece.2019.103545.

Jou, S.K., Malek, N.A.N.N., 2016. Characterization and antibacterial activity of chlorhexidine loaded silver-kaolinite. Appl. Clay Sci. 127–128, 1–9. https://doi.org/10.1016/j.clay.2016.04.001.

Kathuria, D., Raul, A.D., Wanjari, P., Bharatam, P.V., 2021. European Journal of Medicinal Chemistry Biguanides : Species with versatile therapeutic applications. Eur. J. Med. Chem. 219, 113378 https://doi.org/10.1016/j.ejmech.2021.113378.

Komarneni, S., Pidugu, R., Hoffbauer, W., Schneider, H., 1999. A synthetic Na-rich mica: Synthesis and characterization by 27Al and 29Si magic angle spinning nuclear magnetic resonance spectroscopy. Clay Clay Miner. 47 (4), 410–416. https://doi.org/10.1346/CCMN.1999.0470403.

Korsmeyer, R.W., Gurny, R., Doelker, E., Buri, P., Peppas, N.A., 1983. Mechanisms of solute release from porous hydrophilic polymers. Int. J. Pharm. 15 (1), 25–35. https://doi.org/10.1016/0378-5173(83)90064-9.

Lin-Vien, D., Colthup, N.B., Fateley, W.G.F., Grasselli, J.G., 1991. The Handbook of Infrared and Raman Characteristic Frequencies of Organic Molecules, vol. 29, Issue 10. Elsevier. https://www.elsevier.com/books/the-handbook-of-infrared-and-raman-characteristic-frequencies-of-organic-molecules/lin-vien/978-0-08-057116-4.

Lobato-Aguilar, H., Uribe-Calderón, J.A., Herrera-Kao, W., Duarte-Aranda, S., Baas-López, J.M., Escobar-Morales, B., Cauich-Rodríguez, J.V., Cervantes-Uc, J.M., 2018. Synthesis, characterization and chlorhexidine release from either montmorillonite or palygorskite modified organoclays for antibacterial applications. J. Drug Deliv. Sci. Technol. 46 (April), 452–460. https://doi.org/10.1016/j.jddst.2018.06.007.

Lobato-Aguilar, H.A., Lizama-Uc, G., Uribe-Calderon, J.A., Cauich-Rodriguez, J., Rodriguez-Fuentes, N., Cervantes-Uc, J.M., 2020. Antibacterial properties and release kinetics of chlorhexidine diacetate from montmorillonite and palygorskite clays. J. Biomater. Appl. 34 (8), 1052–1058. https://doi.org/10.1177/0885328219891710.

Madejová, J., Gates, W.P., Petit, S., 2017. IR Spectra of Clay Minerals. In: Gates, F.B.W.P., Kloprogge, J.T., Madejová, J. (Eds.), Developments in Clay Science, vol. 8. Elsevier. https://doi.org/10.1016/B978-0-08-100355-8.00005-9.

Martín, J., del Orta, M.M., Medina-Carrasco, S., Santos, J.L., Aparicio, I., Alonso, E., 2018. Removal of priority and emerging pollutants from aqueous media by adsorption onto synthetic organo-funtionalized high-charge swelling micas. Environ. Res. 164 (January), 488–494. https://doi.org/10.1016/j.envres.2018.03.037.

Martín, J., del Orta, M.M., Medina-Carrasco, S., Santos, J.L., Aparicio, I., Alonso, E., 2019. Evaluation of a modified mica and montmorillonite for the adsorption of ibuprofen from aqueous media. Appl. Clay Sci. 171 (January), 29–37. https://doi.org/10.1016/j.clay.2019.02.002.

Meng, N., Zhou, N.L., Zhang, S.Q., Shen, J., 2009. Controlled release and antibacterial activity chlorhexidine acetate (CA) intercalated in montmorillonite. Int. J. Pharm. 382 (1–2), 45–49. https://doi.org/10.1016/j.ijpharm.2009.08.004.

Oliveira, L.H., de Lima, I.S.S., da Neta, E.R., de Lima, S.G., Trigueiro, P., Osajima, J.A., da Silva-Filho, E.C., Jaber, M., Fonseca, M.G., 2023. Essential oil in bentonite: effect of organofunctionalization on antibacterial activities. Appl. Clay Sci. 245 (October), 107158 https://doi.org/10.1016/j.clay.2023.107158.

Onnainty, R., Onida, B., Páez, P., Longhi, M., Barresi, A., Granero, G., 2016. Targeted chitosan-based bionanocomposites for controlled oral mucosal delivery of chlorhexidine. Int. J. Pharm. 509 (1–2), 408–418. https://doi.org/10.1016/j.ijpharm.2016.06.011.

Osuna, F.J., Cota, A., Fernández, M.A., Pavón, E., Torres Sánchez, R.M., Alba, M.D., 2019a. Influence of framework and interlayer on the colloidal stability of design swelling high-charged micas. Colloids Surf. A Physicochem. Eng. Asp. 561 (October 2018), 32–38. https://doi.org/10.1016/j.colsurfa.2018.09.086.

Osuna, F.J., Pavón, E., Alba, M.D., 2019b. Design swelling micas: Insights on heavy metals cation exchange reaction. Appl. Clay Sci. 182 (September), 105298 https://doi.org/10.1016/j.clay.2019.105298.
Osuna, F.J., Pavón, E., Alba, M.D., 2020. An insight on the design of mercapto functionalized swelling brittle micas. J. Colloid Interface Sci. 561, 533–541. https://doi.org/10.1016/j.jcis.2019.11.028.
Osuna, F.J., Pavón, E., Alba, M.D., 2021. Pb2+, Cd2+ and Hg2+ removal by designed functionalized swelling high-charged micas. Sci. Total Environ. 764, 142811 https://doi.org/10.1016/j.scitotenv.2020.142811.
Pal, S., Yoon, E.J., Tak, Y.K., Choi, E.C., Song, J.M., 2009. Synthesis of highly antibacterial nanocrystalline trivalent silver polydiguanide. J. Am. Chem. Soc. 131 (44), 16147–16155. https://doi.org/10.1021/ja9051125.
Park, M., Lee, D.H., Choi, C.L., Kim, S.S., Kim, K.S., Choi, J., 2002. Pure Na-4-mica: Synthesis and Characterization. Chem. Mater. 14 (6), 2582–2589. https://doi.org/10.1021/cm0116267.
Pazos, M.C., Castro, M.A., Orta, M.M., Pavón, E., Rios, J.S.V., Alba, M.D., 2012. Synthetic high-charge organomica: effect of the layer charge and alkyl chain length on the structure of the adsorbed surfactants. Langmuir 28 (19), 7325–7332. https://doi.org/10.1021/la300153e.
Peppas, N.A., Sahlin, J.J., 1989. A simple equation for the description of solute release. III. Coupling of diffusion and relaxation. Int. J. Pharm. 57 (2), 169–172. https://doi.org/10.1016/0378-5173(89)90306-2.
Peraro, G.R., Donzelli, E.H., Oliveira, P.F., Tavares, D.C., Gomes Martins, C.H., Molina, E. F., de Faria, E.H., 2020. Aminofunctionalized LAPONITE® as a versatile hybrid material for chlorhexidine digluconate incorporation: Cytotoxicity and antimicrobial activities. Appl. Clay Sci. 195 (June 2019), 105733 https://doi.org/10.1016/j.clay.2020.105733.
Polli, J.E., Rekhi, G.S., Augsburger, L.L., Shah, V.P., 1997. Methods to compare Dissolution Profiles and a Rationale for Wide Dissolution specifications for Metoprolol Tartrate tablets†. J. Pharm. Sci. 86 (6), 690–700. https://doi.org/10.1021/js960473x.
Saadat, S., Rawtani, D., Parikh, G., 2022. Clay minerals-based drug delivery systems for anti-tuberculosis drugs. J. Drug Deliv. Sci. Technol. 76, 103755 https://doi.org/10.1016/J.JDDST.2022.103755.
Saha, K., Butola, B.S., Joshi, M., 2014. Synthesis and characterization of chlorhexidine acetate drug-montmorillonite intercalates for antibacterial applications. Appl. Clay Sci. 101, 477–483. https://doi.org/10.1016/j.clay.2014.09.010.
Samlíková, M., Holešová, S., Hundáková, M., Pazdziora, E., Jankovič, Ľ., Valášková, M., 2017. Preparation of antibacterial chlorhexidine/vermiculite and release study. Int. J. Miner. Process. 159, 1–6. https://doi.org/10.1016/j.minpro.2016.12.002.
Sun, B., Zhang, M., Zhou, N., Chu, X., Yuan, P., Chi, C., Wu, F., Shen, J., 2018. Study on montmorillonite-chlorhexidine acetate-terbinafine hydrochloride intercalation composites as drug release systems. RSC Adv. 8 (38), 21369–21377. https://doi.org/10.1039/c8ra03651a.
Taruta, S., Inoue, T., Miyake, S., Tsubata, A., Kemi, J., 2022. Synthesis and ionic conductivity of novel high charged tetrasilisic type micas. Appl. Clay Sci. 229 (August), 106670 https://doi.org/10.1016/j.clay.2022.106670.
Williamson, D.A., Carter, G.P., Howden, B.P., 2017. Current and emerging topical antibacterials and antiseptics: Agents, action, and resistance patterns. In. Clin. Microbiol. Rev. 30, Issue 3, 827–860. https://doi.org/10.1128/CMR.00112-16.
Wu, Y., Zhou, N., Li, W., Gu, H., Fan, Y., Yuan, J., 2013. Long-term and controlled release of chlorhexidine-copper(II) from organically modified montmorillonite (OMMT) nanocomposites. Mater. Sci. Eng. C 33 (2), 752–757. https://doi.org/10.1016/j.msec.2012.10.028.
Wu, Y., Yang, Y., Liu, H., Yao, X., Leng, F., Chen, Y., Tian, W., 2017. Long-term antibacterial protected cotton fabric coating by controlled release of chlorhexidine gluconate from halloysite nanotubes. RSC Adv. 7 (31), 18917–18925. https://doi.org/10.1039/c7ra01464c.
Wu, S.C., Liu, F., Zhu, K., Shen, J.Z., 2019. Natural Products that Target Virulence Factors in Antibiotic-Resistant Staphylococcus aureus. J. Agric. Food Chem. 67 (48), 13195–13211. https://doi.org/10.1021/acs.jafc.9b05595.
Xu, W., Gao, Q., Xu, Y., Wu, D., Sun, Y., Shen, W., Deng, F., 2009. Controllable release of ibuprofen from size-adjustable and surface hydrophobic mesoporous silica spheres. Powder Technol. 191 (1–2), 13–20. https://doi.org/10.1016/j.powtec.2008.09.001.
Yang, D., Yuan, P., Zhu, J.X., He, H.P., 2007. Synthesis and characterization of antibacterial compounds using montmorillonite and chlorhexidine acetate. J. Therm. Anal. Calorim. 89 (3), 847–852. https://doi.org/10.1007/s10973-006-8318-3.
Yu, Z., Tang, J., Khare, T., Kumar, V., 2020. The alarming antimicrobial resistance in ESKAPEE pathogens: can essential oils come to the rescue? Fitoterapia 140 (October 2019), 104433. https://doi.org/10.1016/j.fitote.2019.104433.
Zheng, L.-Y., Zhu, J.-F., 2003. Study on antimicrobial activity of chitosan with different molecular weights. Carbohydr. Polym. 54 (4), 527–530. https://doi.org/10.1016/j.carbpol.2003.07.009.
Zhu, Y., Shi, J., Li, Y., Chen, H., Shen, W., Dong, X., 2005. Storage and release of ibuprofen drug molecules in hollow mesoporous silica spheres with modified pore surface. Microporous Mesoporous Mater. 85 (1–2), 75–81. https://doi.org/10.1016/j.micromeso.2005.06.015.